MAX-PLANCK-INSTITUT
FÜR PLASMAPHYSIK

Gyrokinetic simulations of collisionless tearing modes: retained-spectrum dependence and nonlinear toroidal mode coupling

Jincai Ren[1 *], Emanuele Poli[1], Fabien Widmer[1], Xin Wang[1], Thomas Hayward-Schneider[1], Alberto Bottino[1], Alexey Mishchenko[2], Silvio Sergio Cerri[3], Qingquan Yu[1]

[1]Max-Planck-Institut für Plasmaphysik, Garching bei München, Germany
[2]Max-Planck-Institut für Plasmaphysik, Greifswald, Germany
[3]Université Côte d'Azur, Observatoire de la Côte d'Azur, CNRS, Laboratoire Lagrange, Nice, France
* jincai.ren@ipp.mpg.de

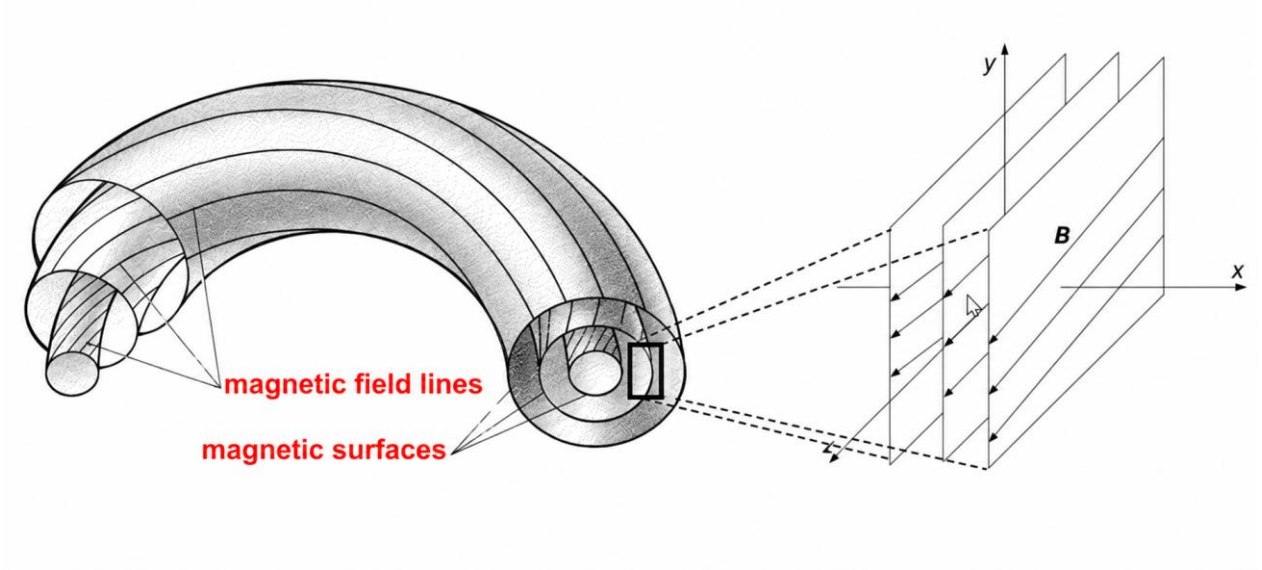
EUROfusion

This work has been carried out within the framework of the EUROfusion Consortium, funded by the European Union via the Euratom Research and Training Programme (Grant Agreement No 101052200 — EUROfusion). Views and opinions expressed are however those of the author(s) only and do not necessarily reflect those of the European Union or the European Commission. Neither the European Union nor the European Commission can be held responsible for them.

Tearing mode in plasmas and gyrokinetic PIC method

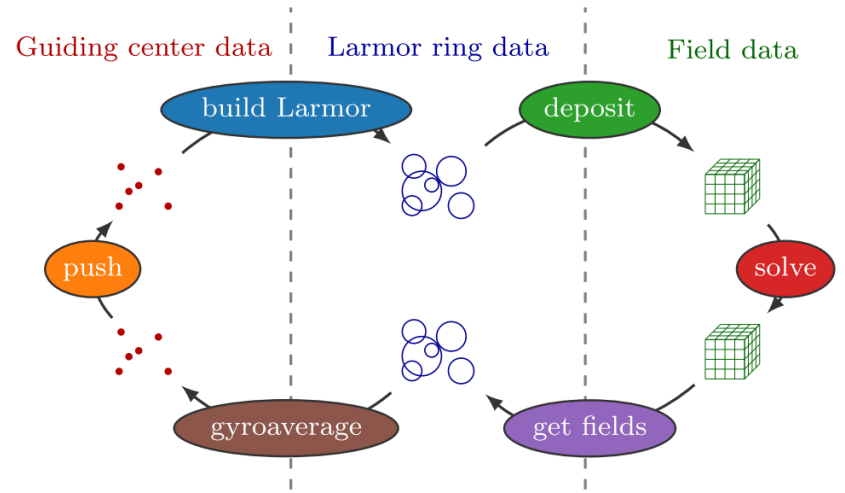
Tearing mode

- Magnetic reconnection
- MHD tearing mode
- Collisionless tearing mode
- Magnetic islands



Gyrokinetic Particle-in-Cell (PIC) method

- Gyrokinetic
- Particle-in-Cell
- ORB5: a global, gyrokinetic, electromagnetic PIC code
- Gyrokinetic ions and drift-kinetic electrons in this work



Main stages of an ORB5 time step. The 6-fold scheme differs from the usual PIC 4-fold scheme because of the introduction of the Larmor ring data

[N. Ohana et al., CPC (2021)]

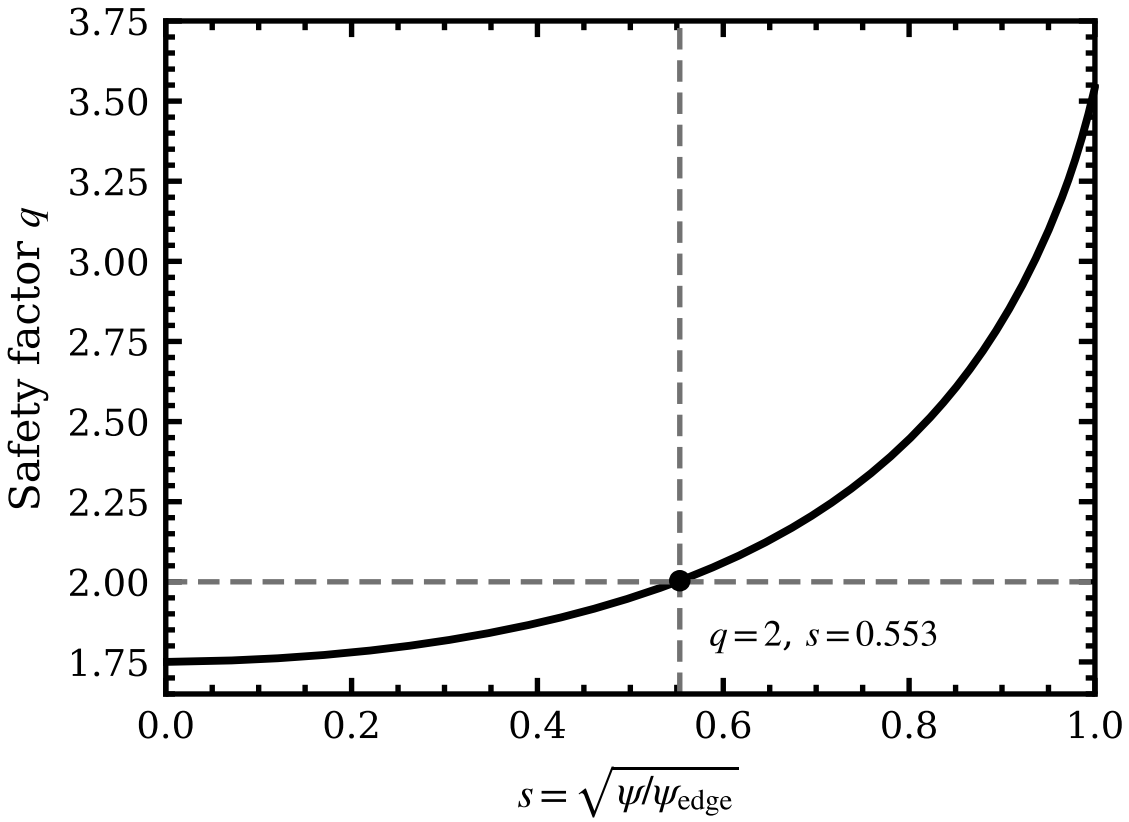
Collisionless tearing mode simulation using ORB5

Equilibrium and simulation setup

- Circular cross-section tokamak geometry
- Flat pressure profile ($\nabla T = \nabla \rho = 0$), β = 5E-4
- Resolution: electron skin depth resolved
- $n \in [0\ 30]$, $m \in [nq-\Delta m, nq+\Delta m]$, $\Delta m = 5$
- nptot = 4E8 (for each species)
- Nonlinear simulation
- Current density gradient driven

$$J_{\parallel} = J_0 \left(1 - \frac{r^2}{a^2}\right)^{\zeta}, \quad \zeta = 1$$

$$q(r) = q_a \frac{r^2/a^2}{1 - (1 - r^2/a^2)^{\zeta+1}}$$

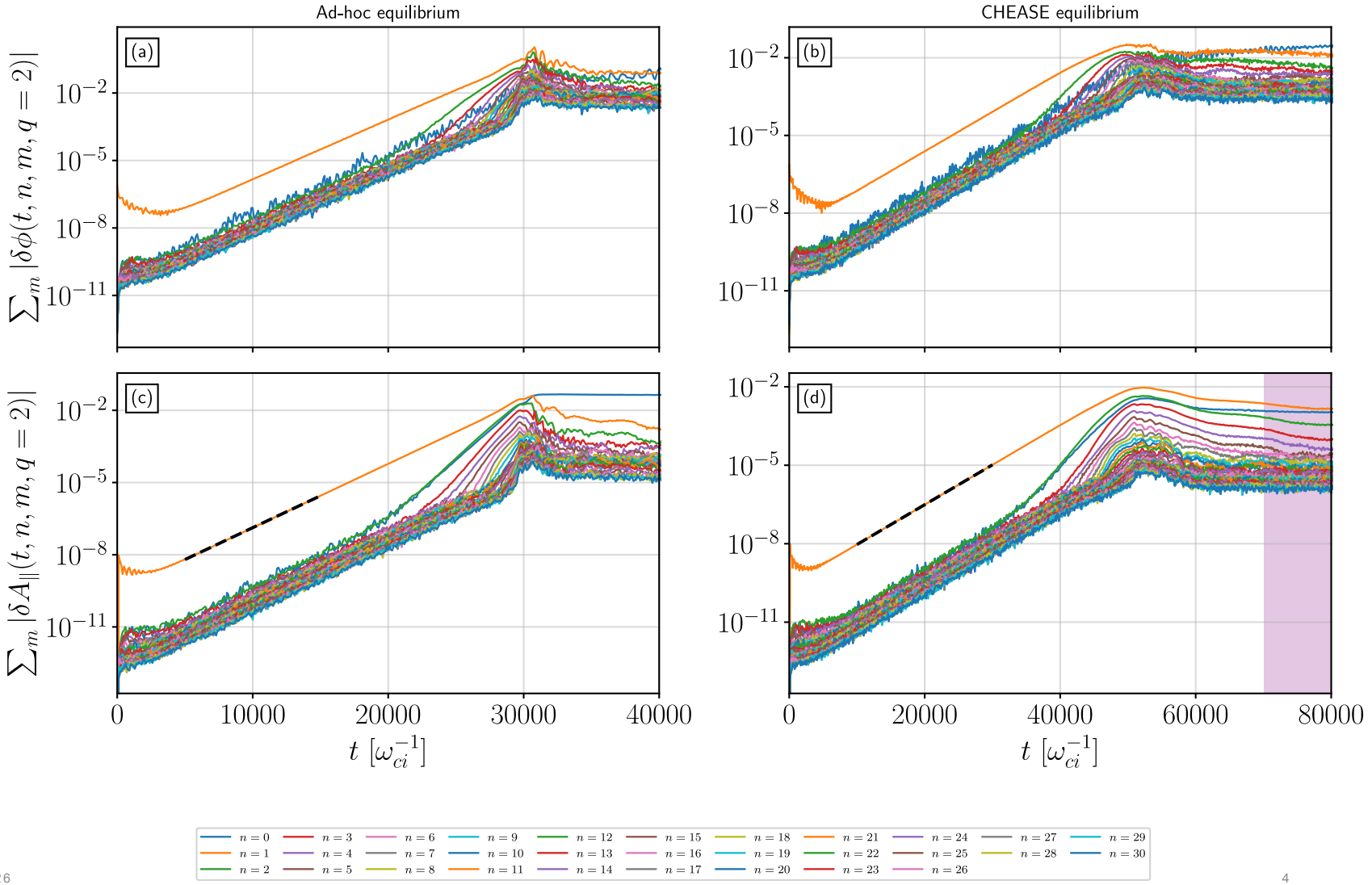


Safety factor q profile

Equilibrium and parameter dependence of the tearing mode

Analytical equilibrium vs CHEASE equilibrium

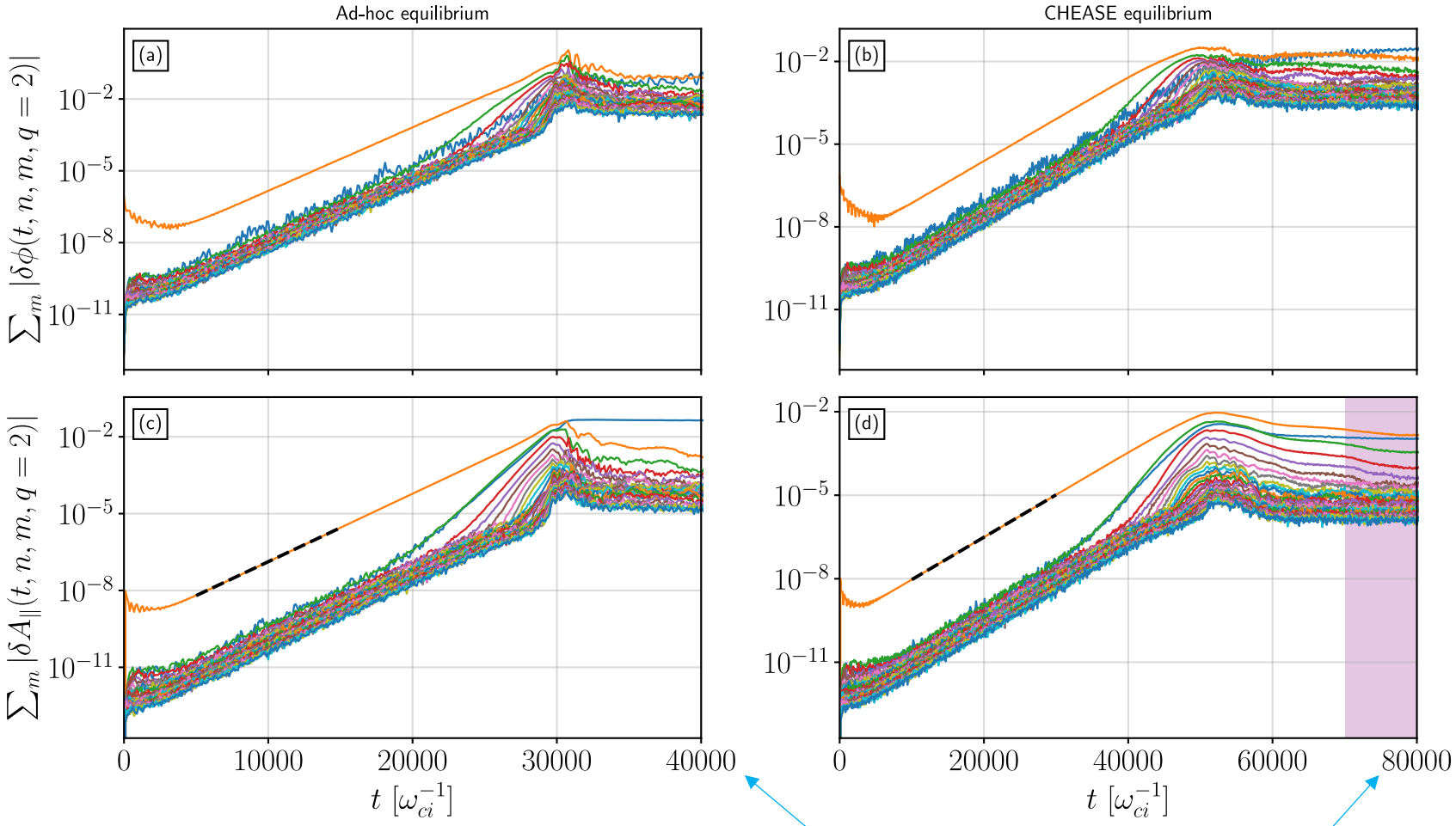
- Aspect ratio R_0/a = 3,
  m_i/m_e=200
- Growth rate
  $\gamma\ (2/1)_{chease}$ = 3.51 E-4ω_{ci}
  $\gamma\ (2/1)_{ad\text{-}hoc}$ = 6.11 E-4 ω_{ci}
- First peak time
  ad-hoc: $t \approx$ 3.0E4 ω_{ci}^{-1}
  chease: $t \approx$ 5.21E4 ω_{ci}^{-1}



Equilibrium and parameter dependence of the tearing mode

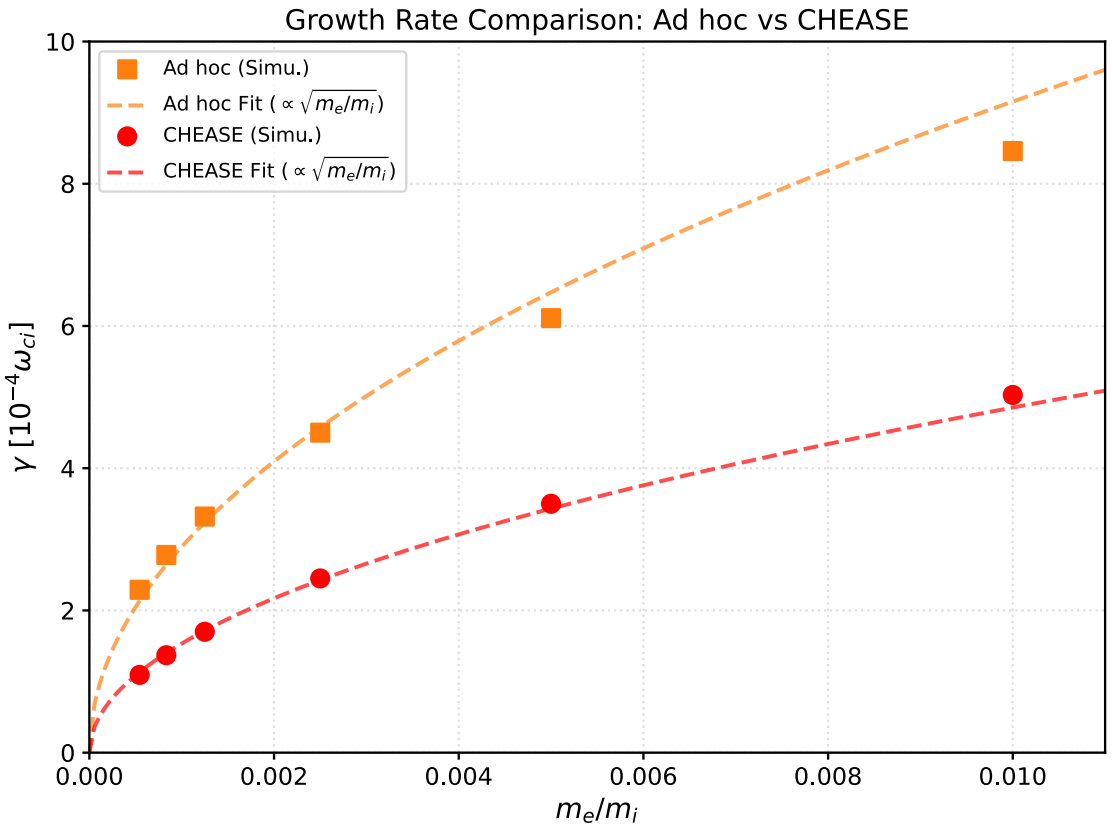
Analytical equilibrium vs CHEASE equilibrium

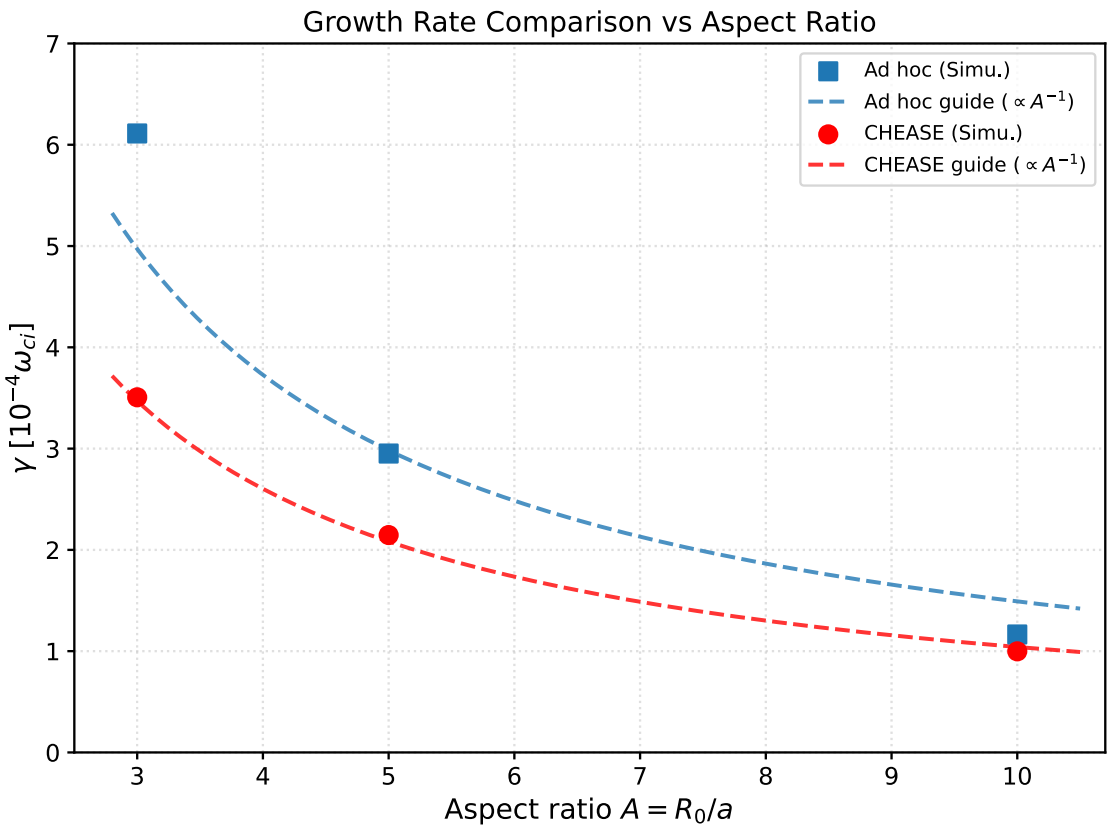
- Aspect ratio R_0/a = 3,
  m_i/m_e=200
- Growth rate
  $\gamma\ (2/1)_{chease}$ = 3.51 E-4ω_{ci}
  $\gamma\ (2/1)_{ad\text{-}hoc}$ = 6.11 E-4 ω_{ci}
- First peak time
  ad-hoc: $t \approx$ 3.0E4 ω_{ci}^{-1}
  chease: $t \approx$ 5.21E4 ω_{ci}^{-1}



Equilibrium and parameter dependence of the tearing mode

Growth rate comparison and benchmark





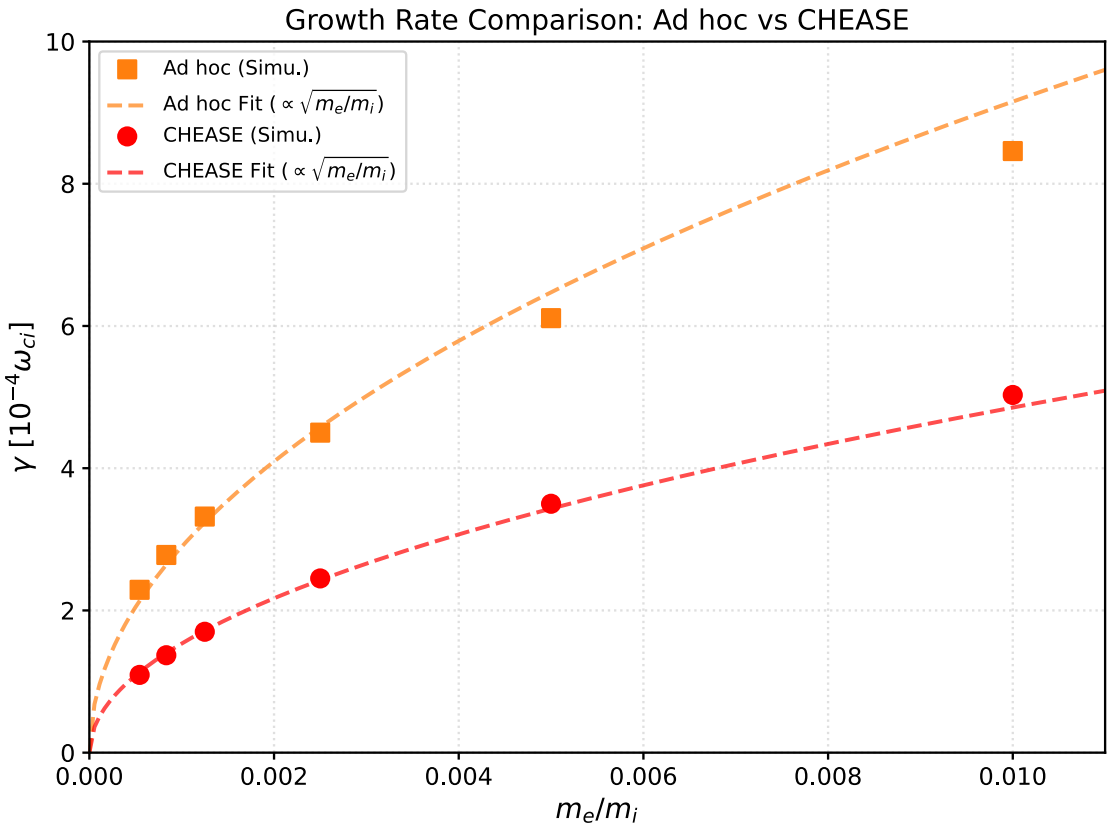
$$\frac{\gamma}{\omega_{ci}} = \Delta' k_\theta k_r \rho_s^3 \frac{B_\theta}{B_\phi} \left(1 + \frac{T_i}{T_e}\right)^{1/2} \left(\frac{m_e}{m_i}\right)^{1/2} \frac{1}{\beta_e}$$

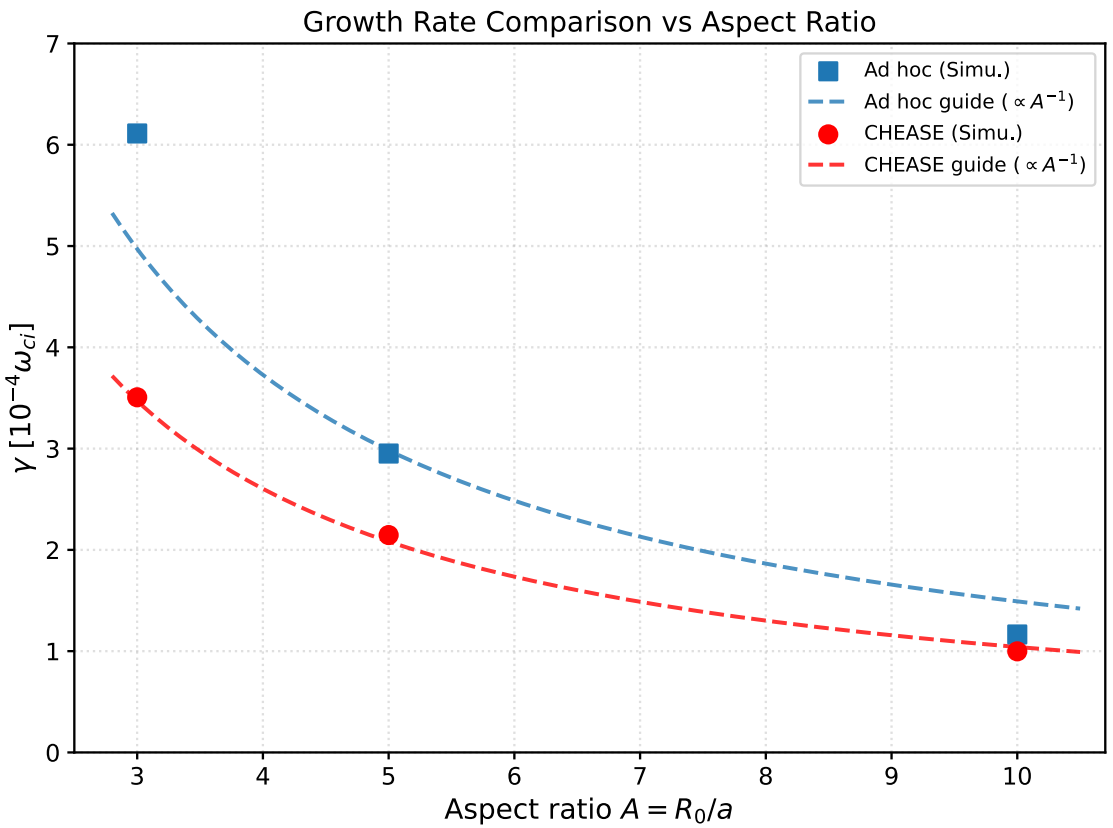
$$\frac{\gamma}{\omega_{ci}} \propto \frac{r}{q} \left(\frac{R_0}{a}\right)^{-1}$$

[Widmer et al, PoP, 2024]

Equilibrium and parameter dependence of the tearing mode

Growth rate comparison and benchmark





$$\frac{\gamma}{\omega_{ci}} = \Delta' k_\theta k_r \rho_s^3 \frac{B_\theta}{B_\phi} \left(1 + \frac{T_i}{T_e}\right)^{1/2} \left(\frac{m_e}{m_i}\right)^{1/2} \frac{1}{\beta_e}$$

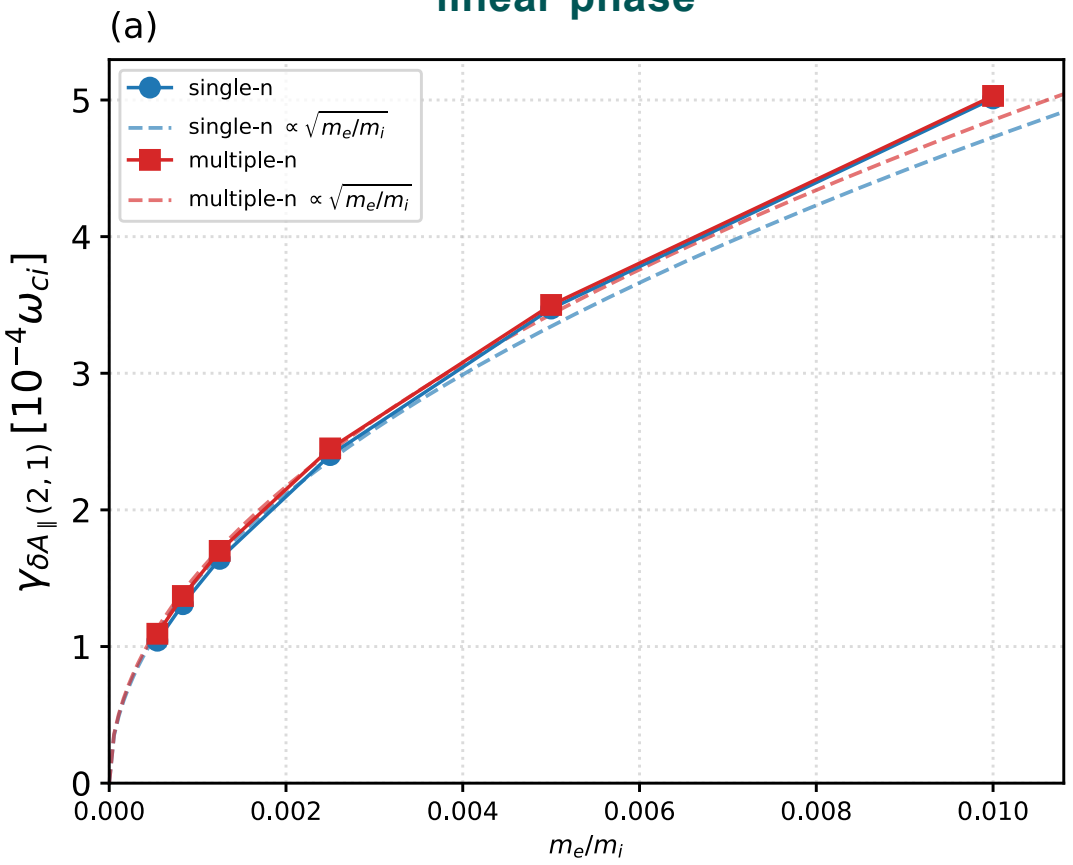
R_0/a = 3 is used in subsequent analyses

[Widmer et al, PoP, 2024]

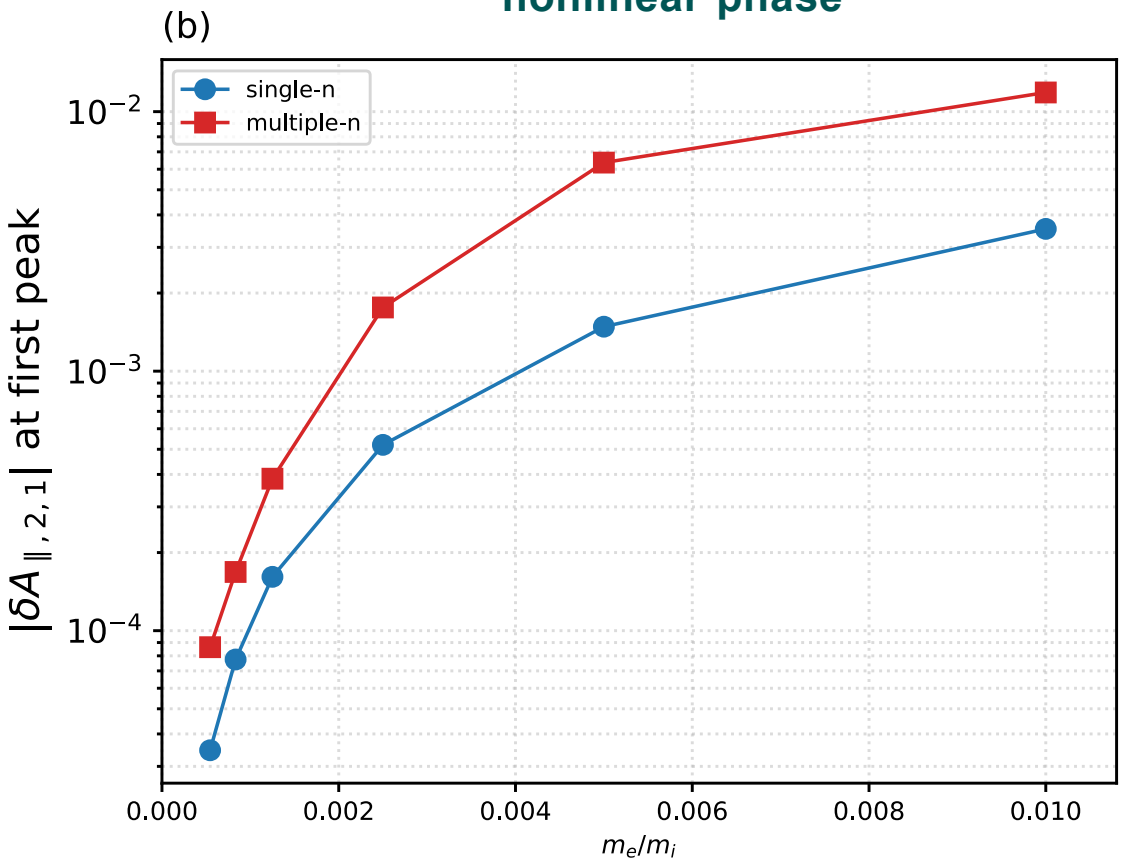
Single-*n* versus multiple-*n* comparison

Primary mode (*n* = 1) growth and saturation in single-n (only *n* = 1 retained) and multiple-*n* (*n* ∈ [0 30]) simulations (chease equilibrium)

linear phase



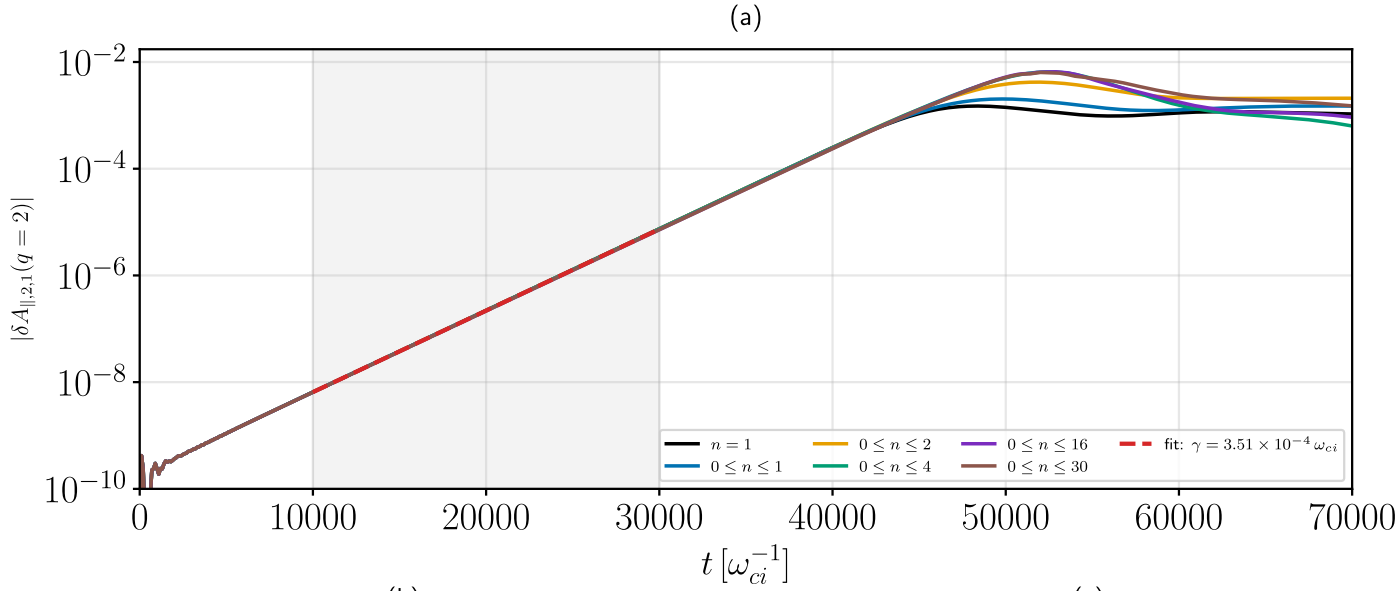
nonlinear phase

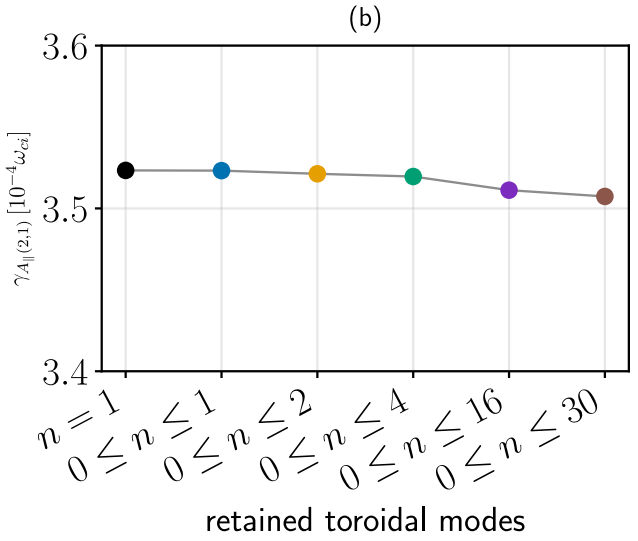


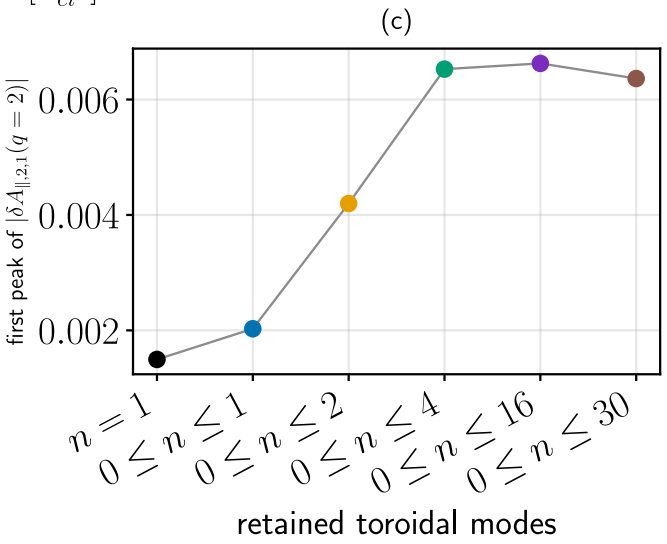
Single-*n* versus multiple-*n* comparison

Primary mode (*n* = 1) growth and saturation with different retained-*n* (chease equilibrium, m_i/m_e=200)

- Little effect on the linear growth rate / linear phase
- Pronounced effect on the nonlinear evolution, especially on the first peak amplitude
- Such effect appears mainly among the low-*n* modes, and the amplitude converges as retained *n* grows



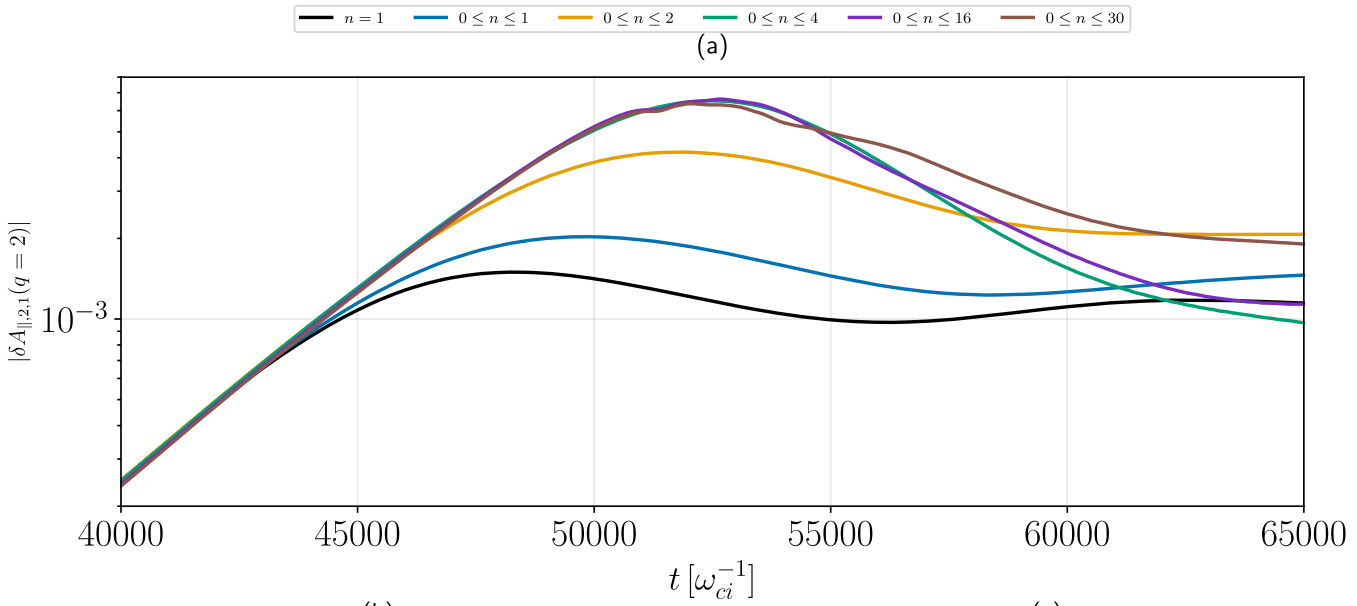


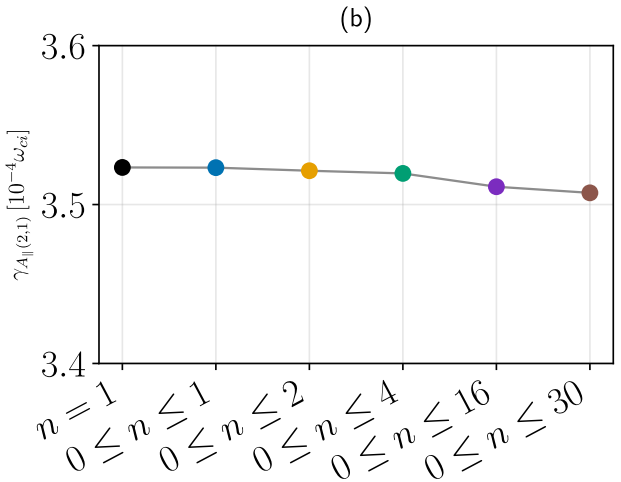


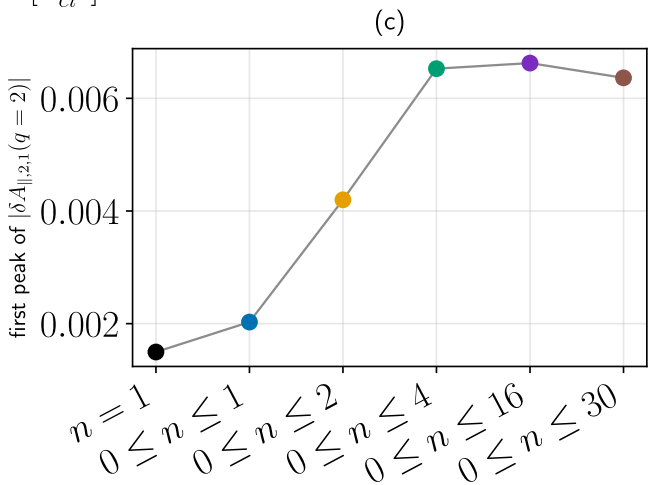
Single-*n* versus multiple-*n* comparison

Primary mode (*n* = 1) growth and saturation with different retained-*n* (chease equilibrium, m_i/m_e=200)

- Little effect on the linear growth rate / linear phase
- Pronounced effect on the nonlinear evolution, especially on the first peak amplitude
- Such effect appears mainly among the low-*n* modes, and the amplitude converges as retained *n* grows



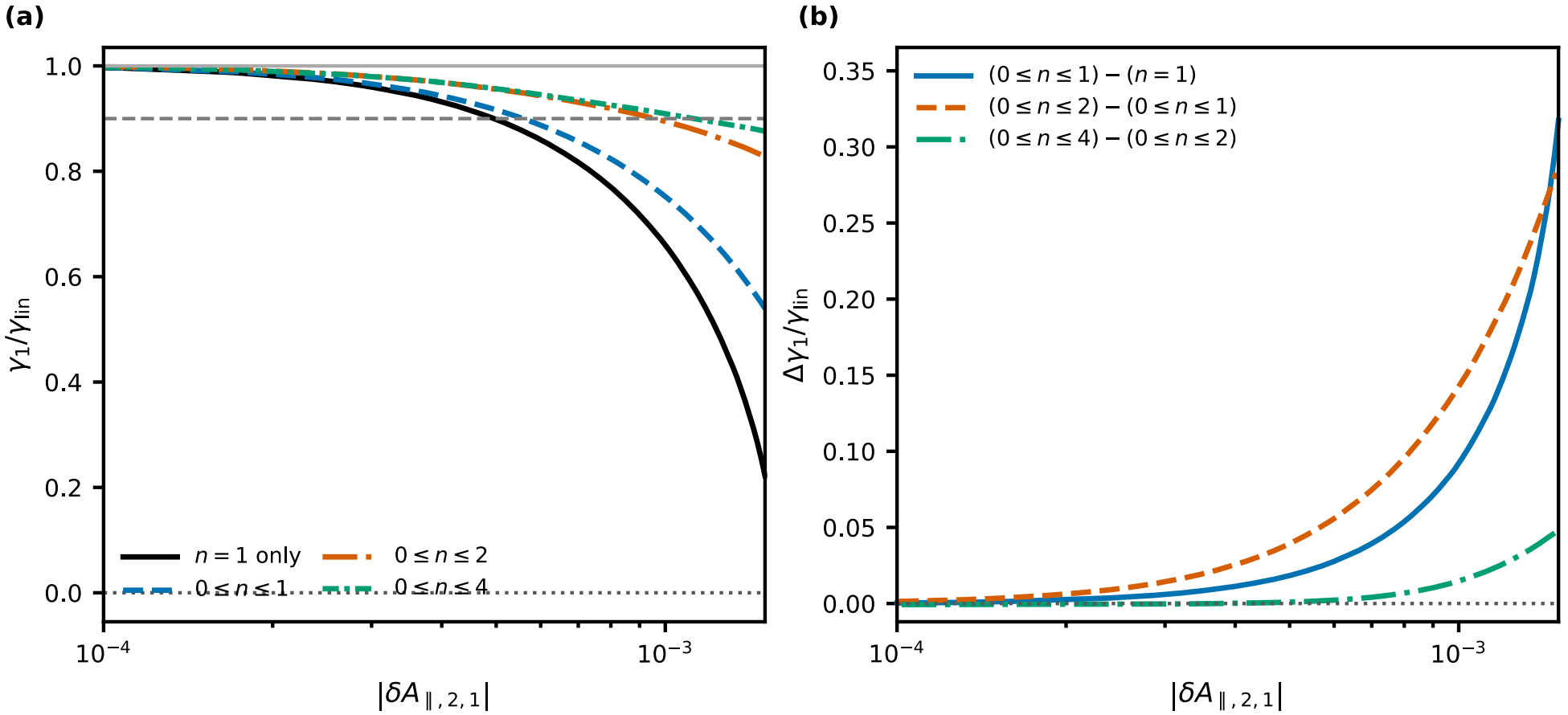




Single-*n* versus multiple-*n* comparison

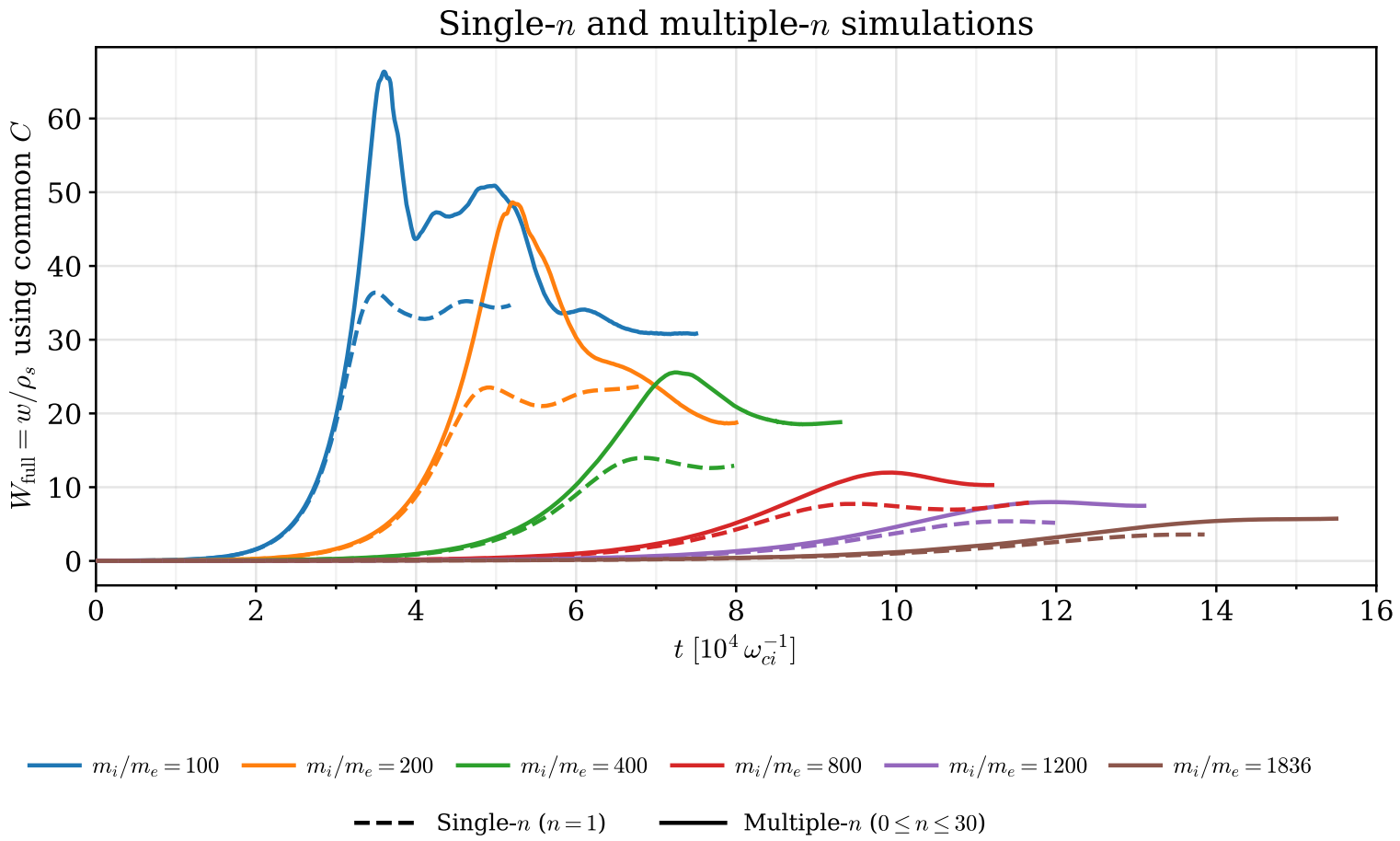
Primary mode (*n* = 1) growth and saturation with different retained-*n* (chease equilibrium, m_i/m_e=200)

$$\gamma_1(t) \equiv \frac{\mathrm{d}\ln(|\delta A_{\parallel,(2,1)}(s_{q=2})|)}{\mathrm{d}t}$$



Single-*n* versus multiple-*n* comparison

Effective primary-island width (chease equilibrium)



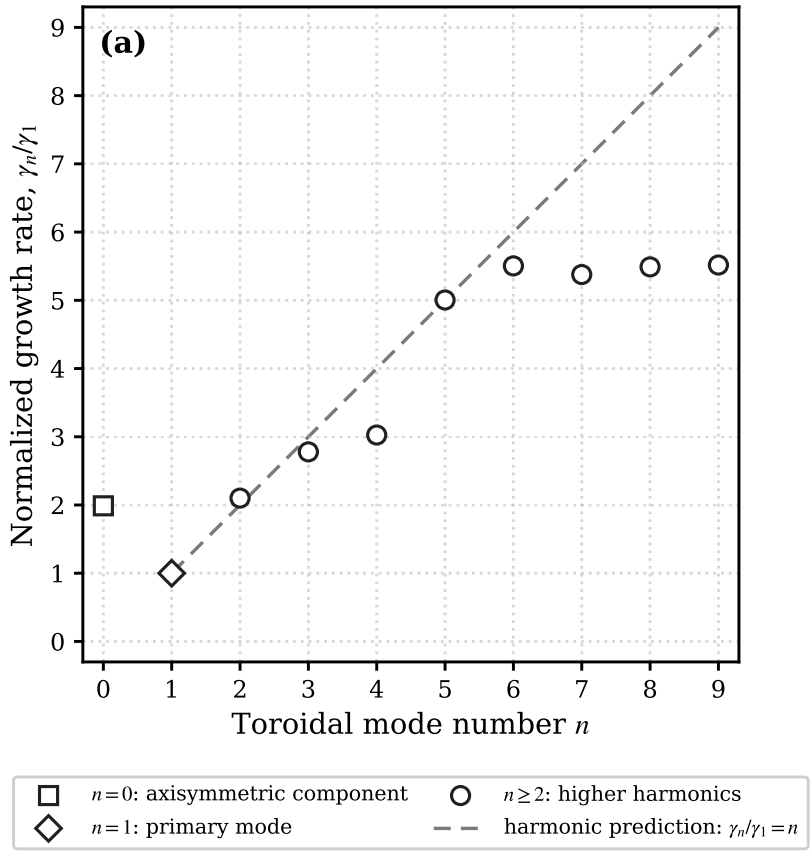
- **Calculated with common-C value**

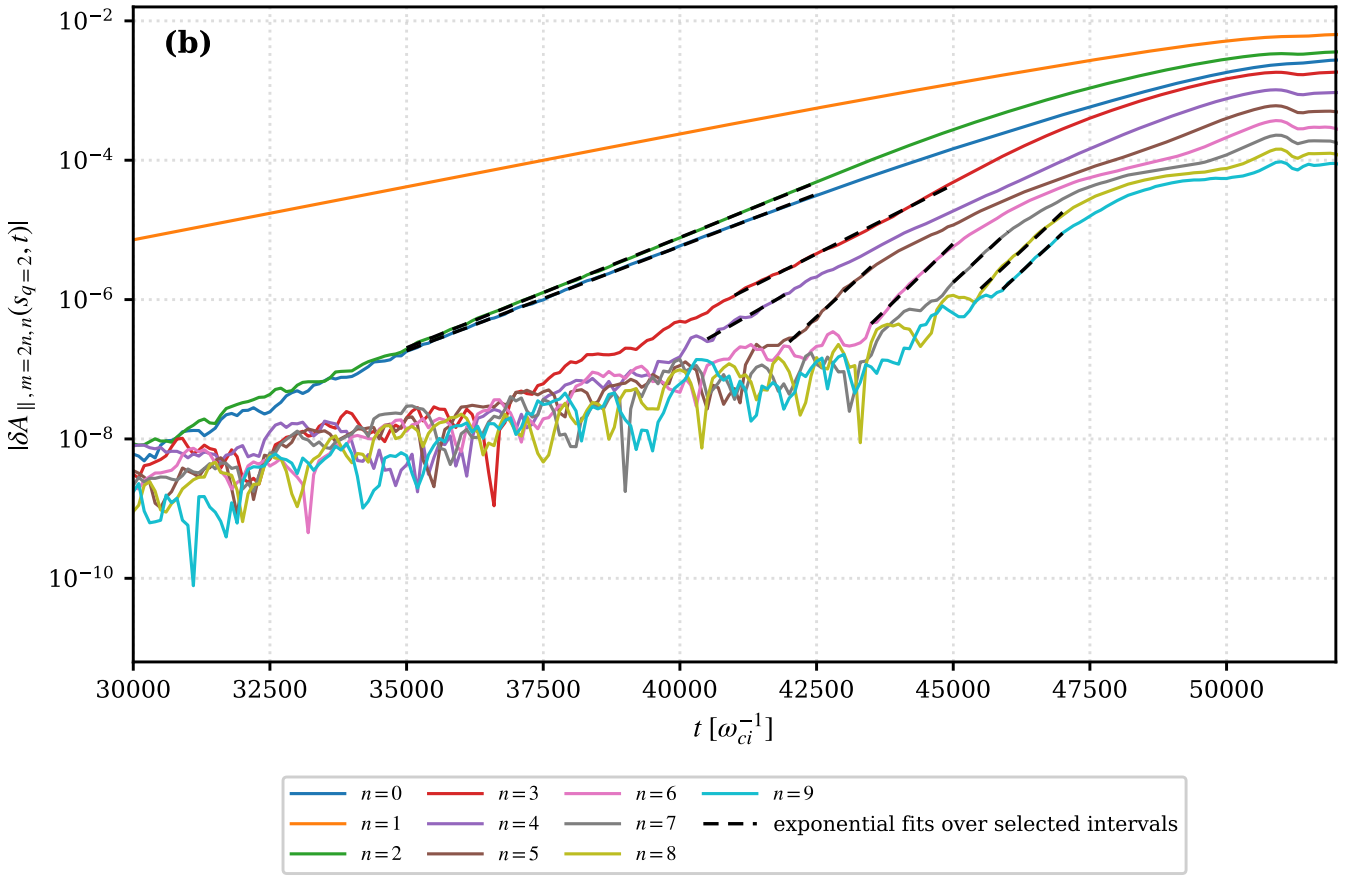
$$W_{\mathrm{full}}(t) \equiv \frac{w(t)}{\rho_s} = C\sqrt{\left|\delta A_{\parallel,2,1}(q=2,t)\right|}$$

- **Larger island width maximum for multiple-*n* simulation at fixed mass ratio**
- **Island width peak decreases as mass ratio increases for both simulation sets**
- **Note the linear scale on the y-axis!**

Mode coupling and toroidal mode spectra

Nonlinear harmonic growth: chease equilibrium, m_i/m_e=200, $n \in [0\ 30]$, R_0/a = 3





Mode coupling and toroidal mode spectra

Toroidal triad phase analysis (chease equilibrium, m_i/m_e=200, $n \in [0\ 30]$, $R_0/a = 3$)

- the complex coefficient of the *n*-th toroidal component as

$$F_n(t) = A_n(t)e^{i\phi_n(t)}$$

- For a signed triad satisfying the Fourier closure

$$n_1 + n_2 = n_3$$

- the corresponding instantaneous third-order complex product is

$$\overline{B}_{123}(t) = F_{n_1}(t)F_{n_2}(t)F^*_{n_3}(t) = A_{n_1}A_{n_2}A_{n_3}e^{i\Theta_{123}}$$

- with the closing phase being

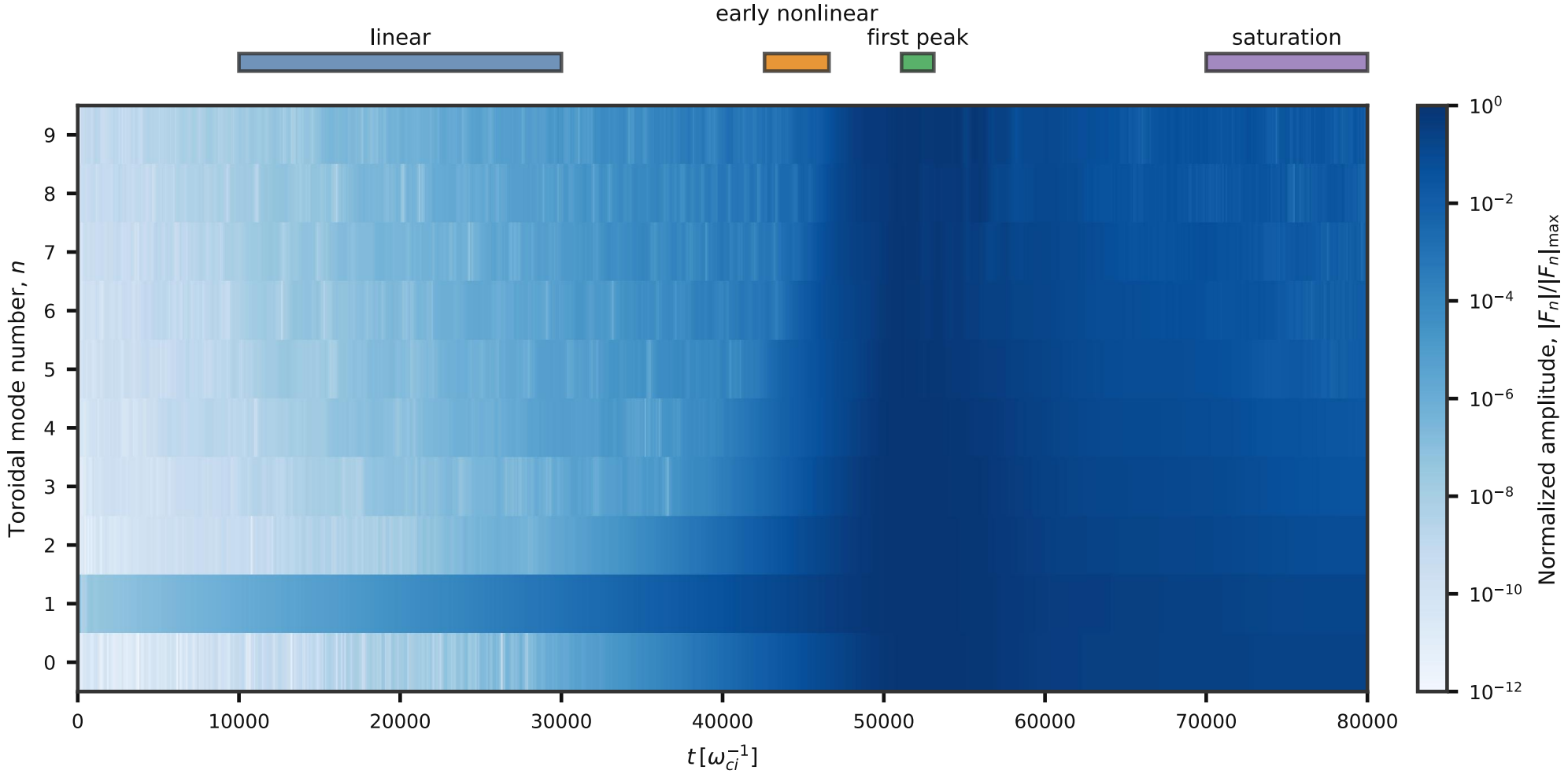
$$\Theta_{123}(t) = \phi_{n_1}(t) + \phi_{n_2}(t) - \phi_{n_3}(t)$$

- Its instantaneous real and imaginary parts are therefore

$$\mathrm{Re}\,\overline{B}_{123} = A_{n_1}A_{n_2}A_{n_3}\cos\Theta_{123}, \qquad \mathrm{Im}\,\overline{B}_{123} = A_{n_1}A_{n_2}A_{n_3}\sin\Theta_{123}$$

Mode coupling and toroidal mode spectra

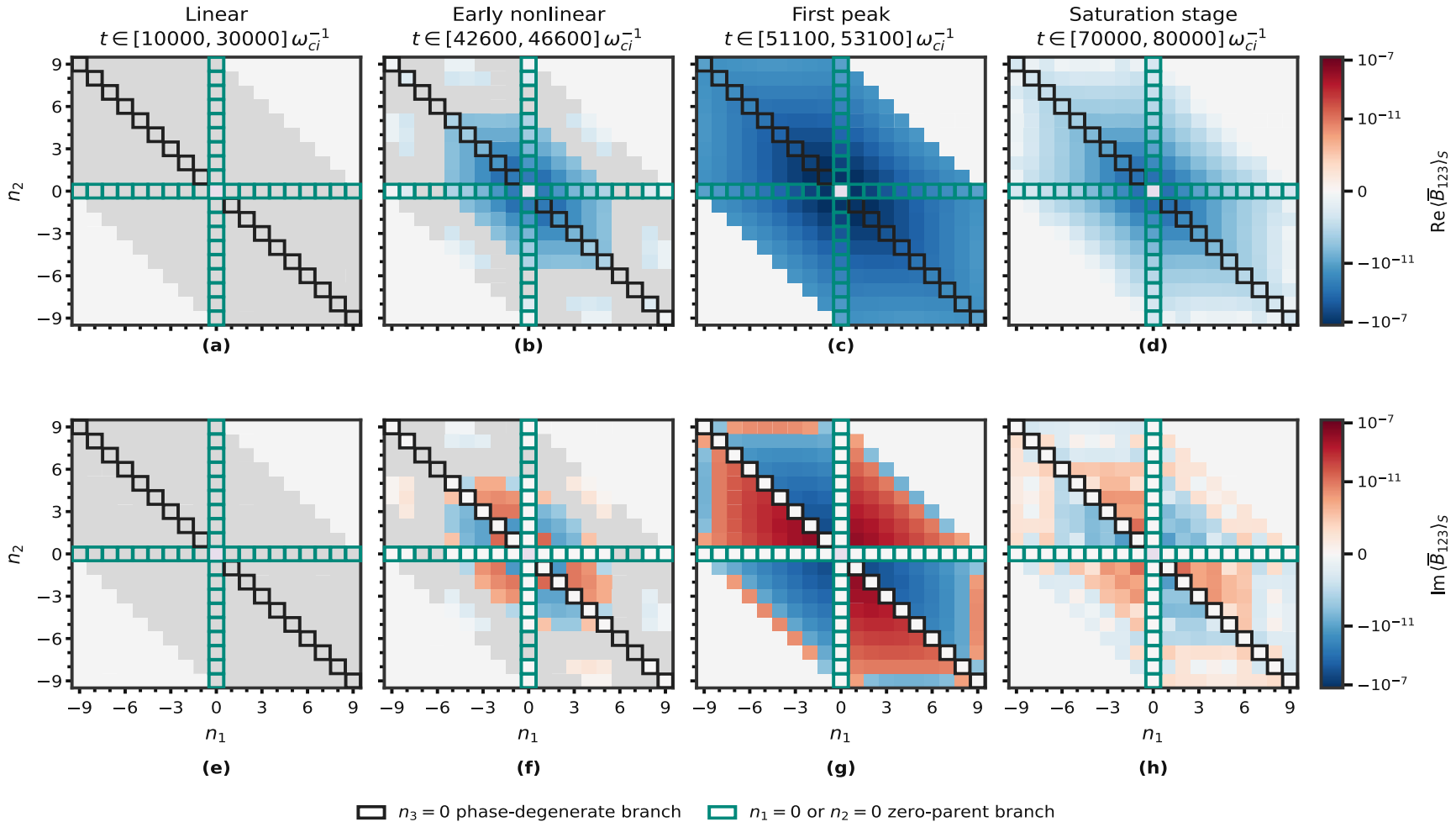
Toroidal triad phase analysis (chease equilibrium, m_i/m_e=200, $n \in [0\ 30]$, R_0/a = 3)



Mode coupling and toroidal mode spectra

Toroidal triad phase analysis

- **Real and imaginary parts of the third-order complex product**
- **Temporal average during the four phases**
- **Negative *n* is reconstructed using**
  $$F_{-n} = F_n^*$$
- **Mode coupling appears and becomes stronger during the nonlinear phase**



Mode coupling and toroidal mode spectra

Toroidal triad phase analysis

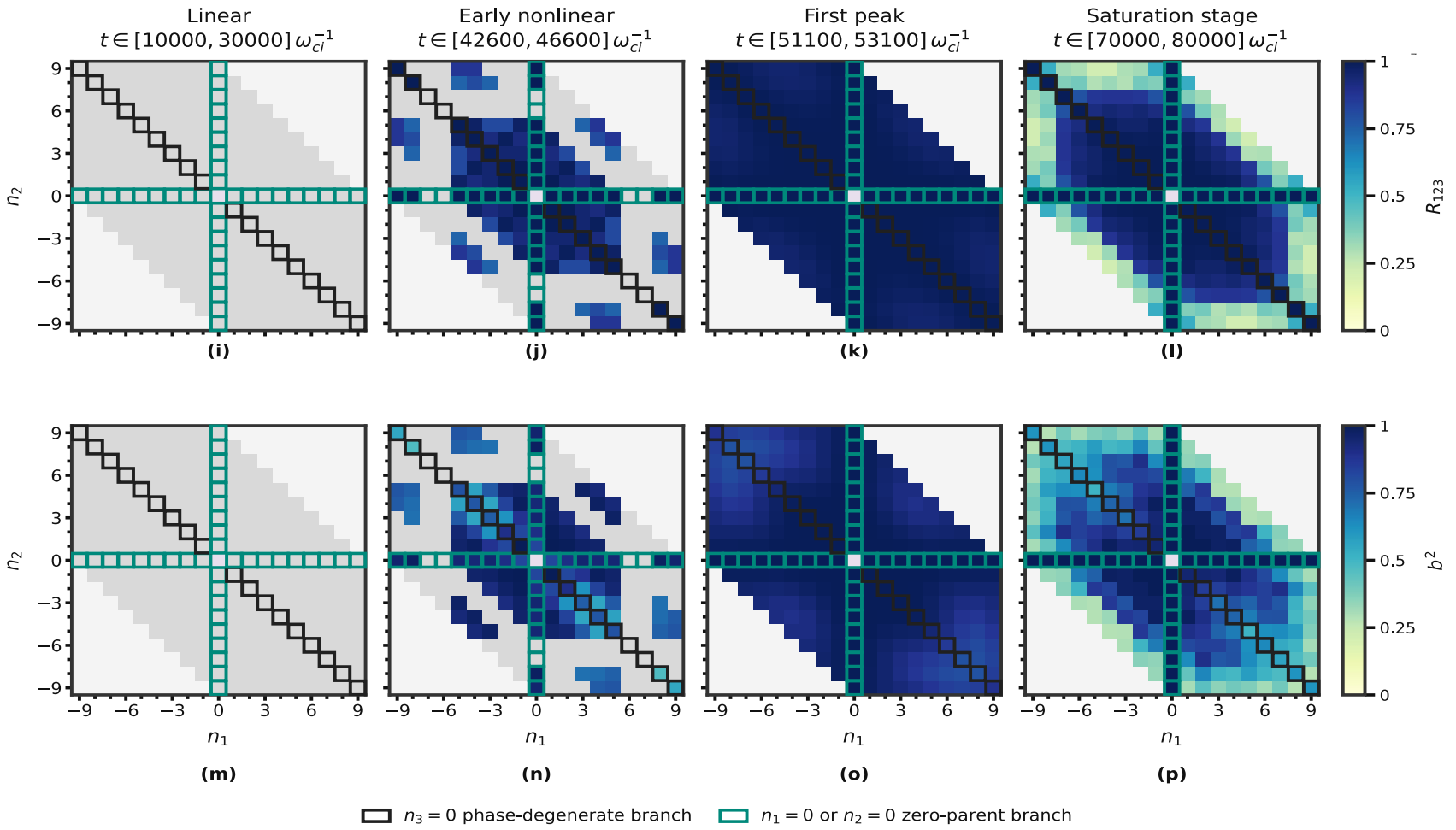
- **Phase relationship and coherence**

$$R_{123} = \left| \left\langle e^{i\Theta_{123}} \right\rangle_S \right|$$

$$b^2_{123} = \frac{\left| \left\langle F_{n_1} F_{n_2} F^*_{n_3} \right\rangle_S \right|^2}{\left\langle |F_{n_1} F_{n_2}|^2 \right\rangle_S \left\langle |F_{n_3}|^2 \right\rangle_S}$$

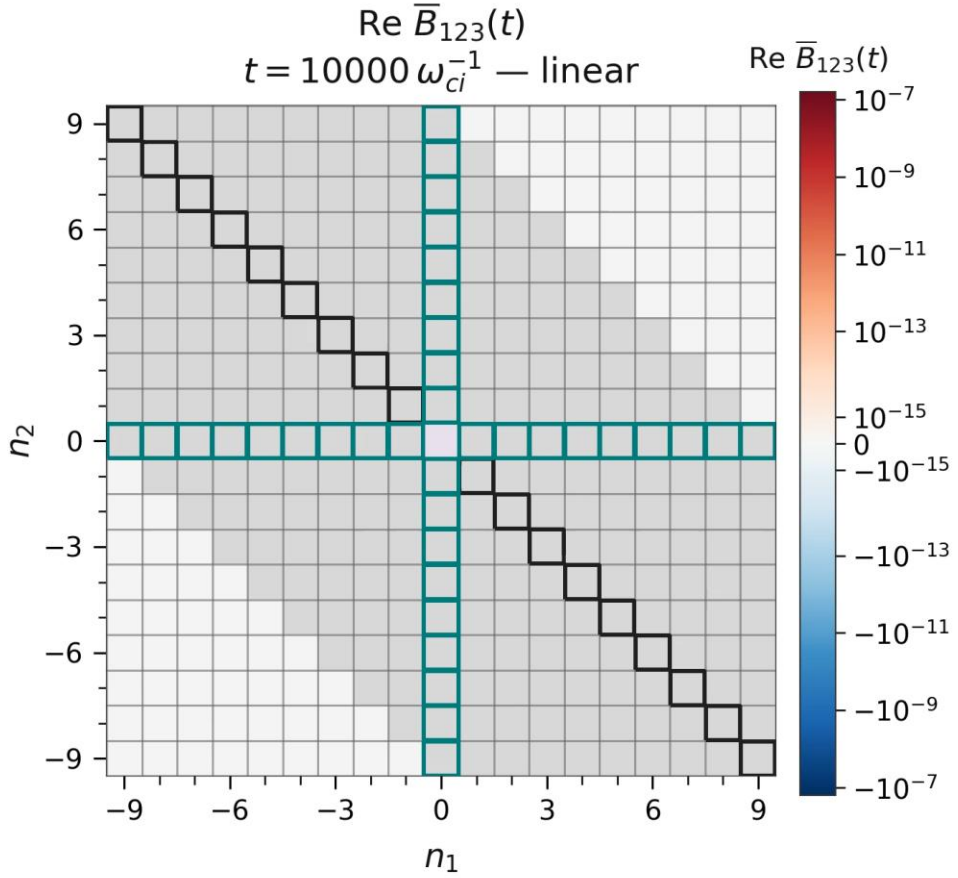
- **Temporal average during the four phases**

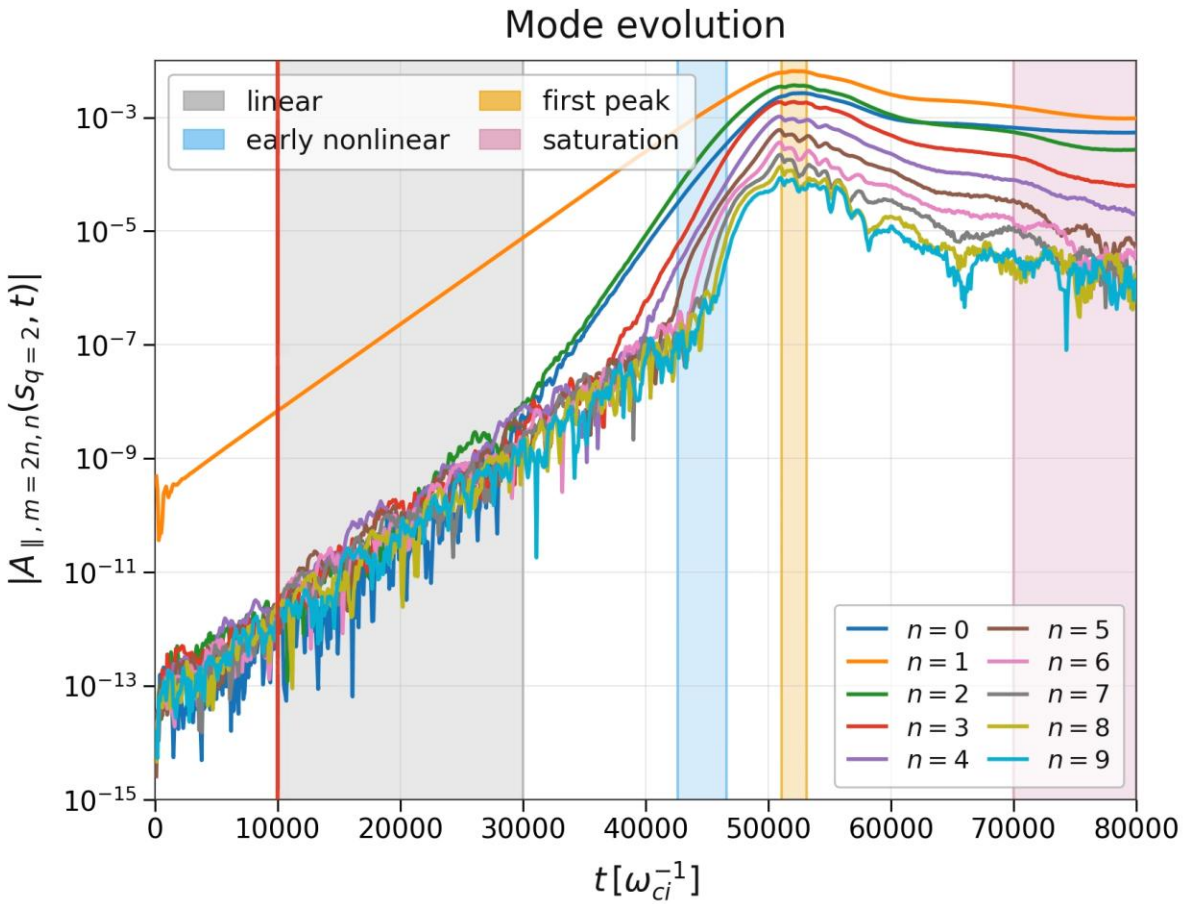
- **Mode coupling appears and becomes stronger during the nonlinear phase**



Mode coupling and toroidal mode spectra

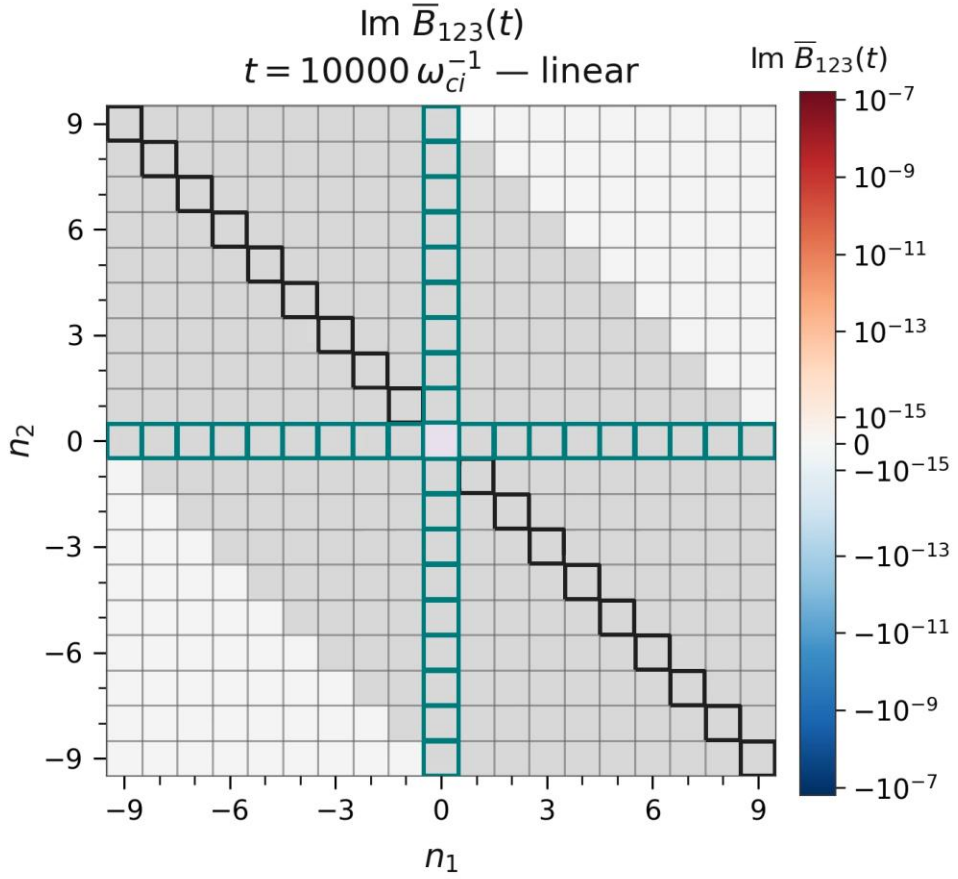
Toroidal triad phase analysis: real part of the third-order complex product

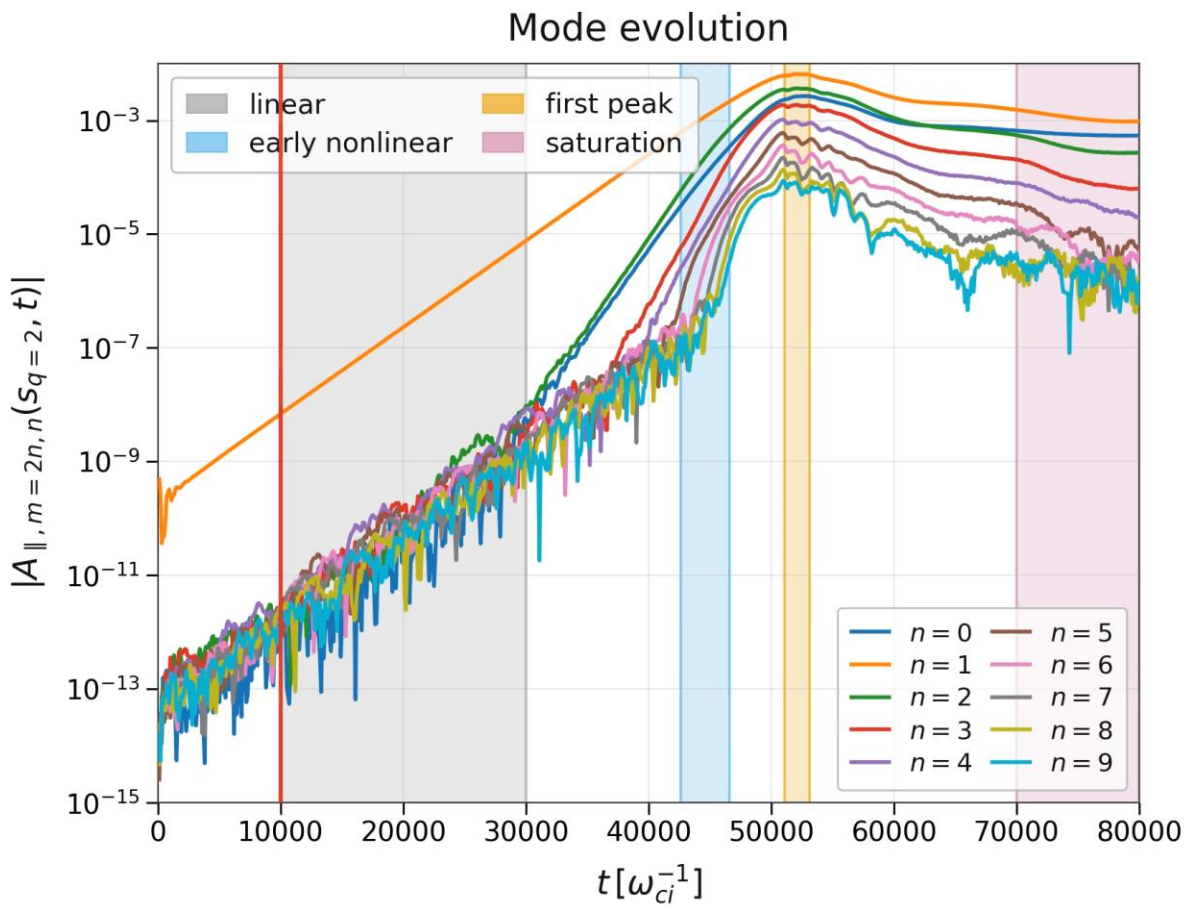




Mode coupling and toroidal mode spectra

Toroidal triad phase analysis: imaginary part of the third-order complex product

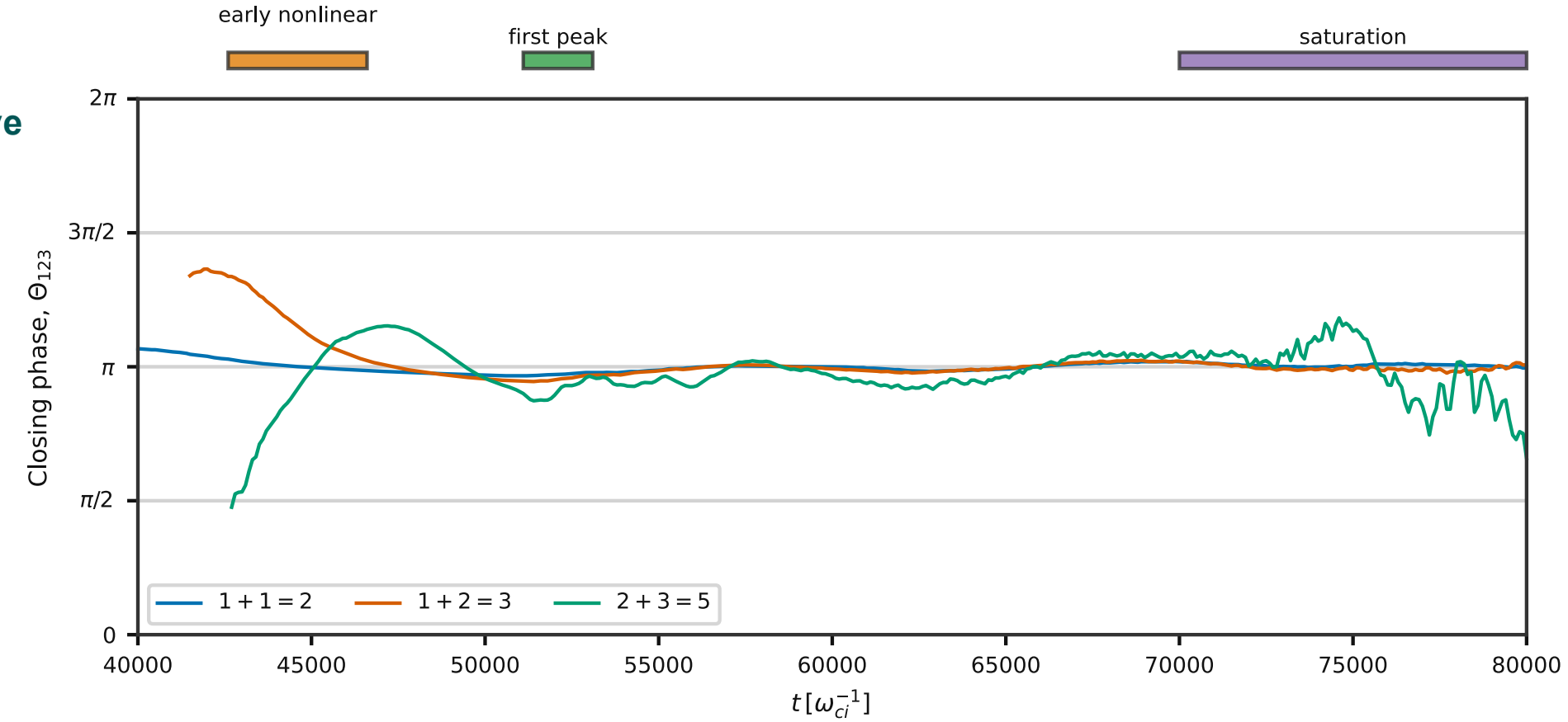




Mode coupling and toroidal mode spectra

Toroidal triad phase analysis

- **Three representative mode coupling samples**
- **Phase lock**



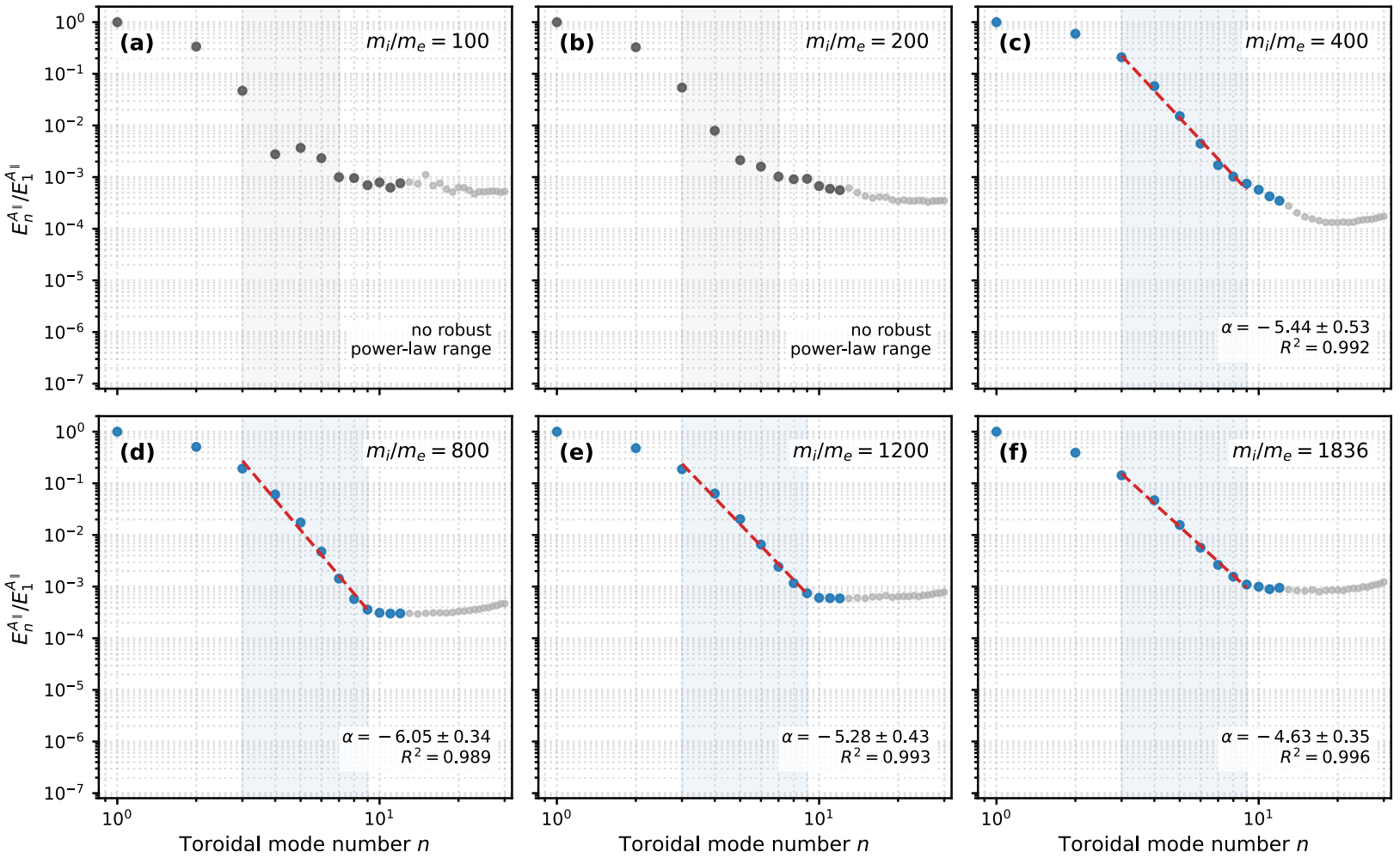
Mode coupling and toroidal mode spectra

Saturation-stage toroidal mode spectra (chease equilibrium, $n \in [0\ 30]$, $R_0/a = 3$)

$$\delta B_\perp \sim k_\perp \delta A_\parallel \sim (m/r)\delta A_\parallel \sim (nq/r)\delta A_\parallel$$

$$E_n^{A_\parallel} = n^2 \sum_m |\delta A_{\parallel,mn}(q=2)|^2$$

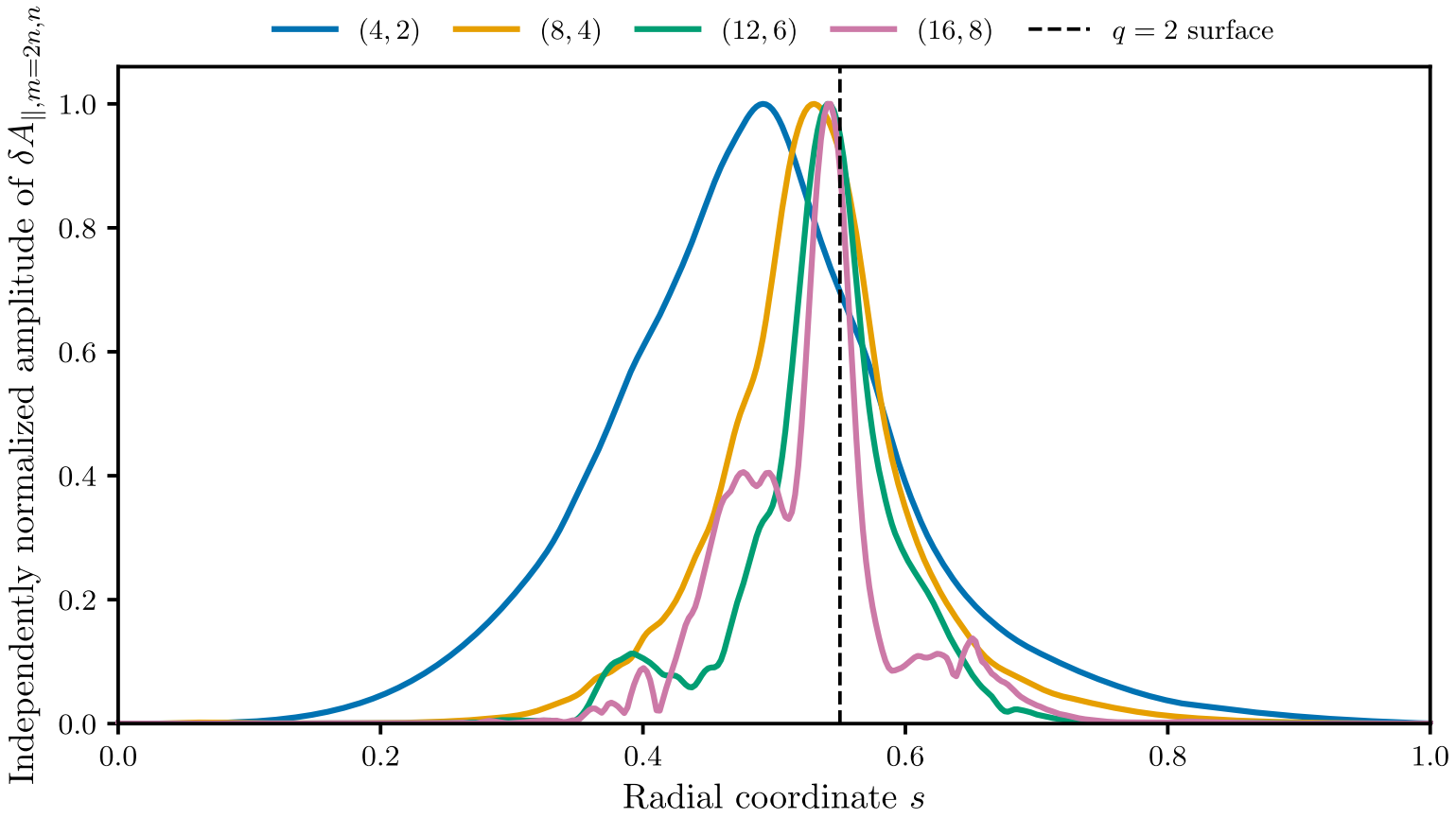
- Normalized E_n spectra at the $q = 2$ surface for the $R_0/a = 3$ under various mass ratios during the saturation stage
- Power-law for $n \in [3\ \ 9]$ resolved approximately for cases $m_i/m_e \geq 400$



Mode coupling and toroidal mode spectra

Radial structures of selected *q*=2 resonant harmonics

- Time-averaged radial structures during the saturation phase
- Each radial profile is **normalized** independently by its maximum



Mode coupling and toroidal mode spectra

Resonant poloidal content and radial parity at q=2 (time-averaged during saturation stage)

- **Local poloidal fraction**

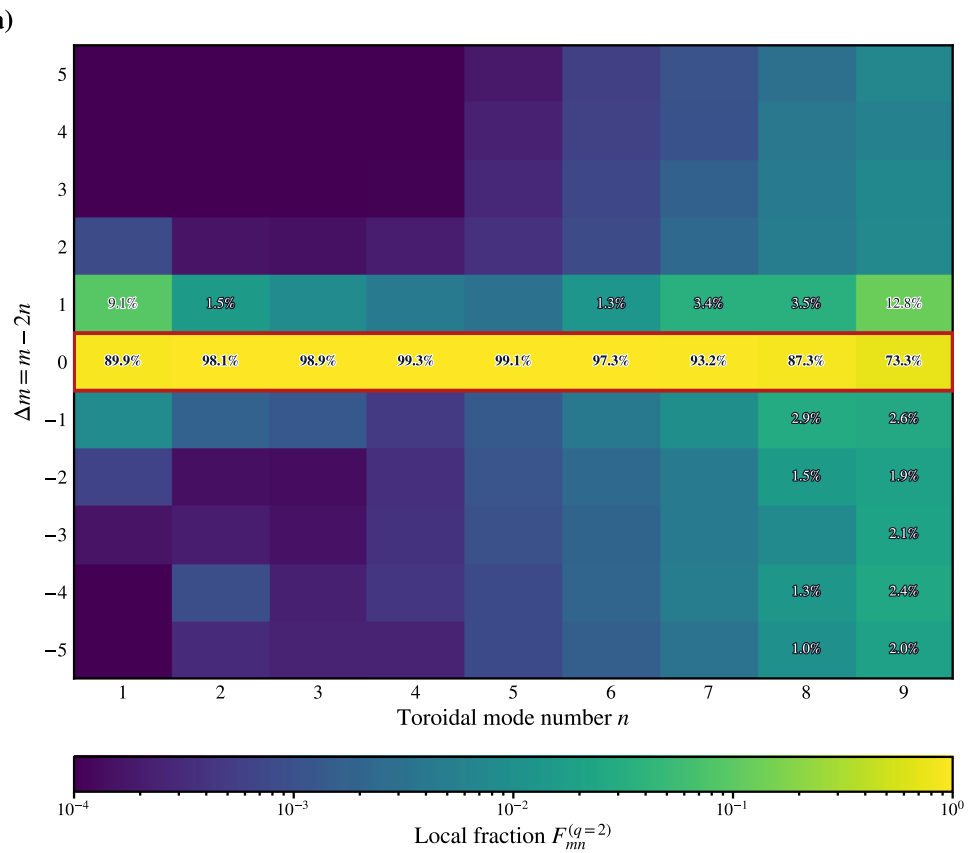
$$F_{mn}^{(q=2)} = \frac{\left\langle |\delta A_{\parallel,mn}(s_{q=2},t)|^2 \right\rangle_t}{\sum_{m'} \left\langle |\delta A_{\parallel,m'n}(s_{q=2},t)|^2 \right\rangle_t}$$

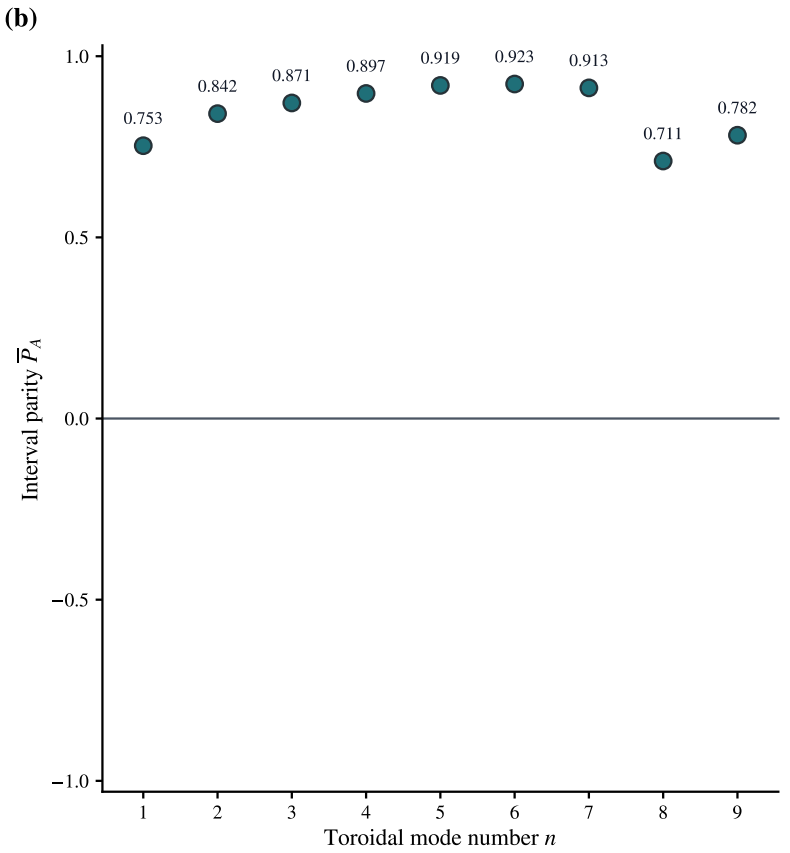
- **Radial parity index**

$$\overline{P}_A(n) = \frac{\sum_t [E_{\mathrm{even}}(n,t) - E_{\mathrm{odd}}(n,t)]}{\sum_t [E_{\mathrm{even}}(n,t) + E_{\mathrm{odd}}(n,t)]}$$

$\overline{P}_A \to +1$: even, tearing-like

$\overline{P}_A \to -1$: odd, twisting-like





Summary

Nonlinear electromagnetic gyrokinetic particle-in-cell simulations using ORB5 were performed to investigate the evolution of a collisionless (*m*,*n*) = (2,1) tearing mode

➢ 1. Linear phase

- Comparison of ad-hoc and CHEASE equilibria
- Growth-rate scaling compared with theoretical predictions
- Effects of aspect ratio and equilibrium geometry

➢ 2. Effect of the retained toroidal-mode spectrum

- Nearly unchanged linear growth rates across different retained spectra
- Strong dependence of the first nonlinear amplitude peak on the retained spectrum
- Calibrated effective magnetic-island width

➢ 3. Nonlinear mode coupling in multiple-*n* simulations

- Stage-resolved triad analysis and phase organization of low-order harmonics
- Saturation-stage toroidal mode spectra and their dependence on the ion-to-electron mass ratio

Ongoing work and future outlook

➢ **Higher-fidelity simulations (test run completed; production run underway)**

- Shaped equilibria with positive or negative triangularity
- Nonuniform density and temperature profiles
- Equilibria containing both $q = 1.5$ and $q = 2$ rational surfaces

➢ **Multiscale interactions between magnetic islands and microturbulence (ongoing)**

- magnetic islands in the inner radial region and microturbulence in the outer region

➢ **Diagnostic development (completed)**

- Test-particle dynamics and energization; Poincaré plot

➢ **ORB5 collision-operator development (for discussion)**

- Review the current implementation, outstanding issues, and next steps for verification and validation